ELSEVIER

Journal of Nuclear Materials 252 (1998) 1–12

journal of nuclear materials

Neutron irradiation and intergranular fracture in vanadium–20 wt% titanium alloys undoped and doped with phosphorus and sulfur

J. Kameda *, T.E. Bloomer, A.H. Swanson, D.Y. Lyu [1]

Ames Laboratory, Iowa State University, Ames, IA 50011, USA

Received 5 March 1996; accepted 13 October 1997

Abstract

The mechanical properties and grain boundary composition affected by neutron irradiation (9.8×10^{24} n/m^2: $E > 0.1$ MeV at 438°C) in undoped, P-doped and S-doped V–20 wt% Ti alloys all containing residual C and O have been studied using a small punch testing method and scanning Auger microprobe analysis. Neutron irradiation facilitated heterogeneous formation of intergranular microcracks, not leading to specimen failure, in all undoped and some S-doped specimens. An irradiated undoped alloy indicated ductility loss to a smaller extent than expected from the easy microcracking due to a mixture of intergranular and transgranular macrocracking. The irradiation effect on the ductility varied in the S-doped alloy, while the irradiation exerted a beneficial effect on low temperature ductility in P-doped alloys. Intergranular S segregation in the undoped alloy and S desegregation in the S-doped alloy occurred during the irradiation. Unirradiated and irradiated P-doped alloys exhibited negligible S segregation and much smaller P segregation than the S segregation in the undoped and S-doped alloys. The grain boundary content of C affecting the ductility was remarkably reduced in the irradiated P-doped alloy and S-doped specimens with ductility loss. The ductility loss and improvement observed in the irradiated alloys are interpreted in light of the variations in segregated and precipitated impurities together with hardening behavior. © 1998 Elsevier Science B.V.

1. Introduction

Since vanadium base alloys possess low neutron activation and excellent strength, they are considered as candidate materials for fusion nuclear reactors [1,2]. The mechanical properties of solid solution strengthened vanadium alloys containing Ti, Cr, Nb or Ta are well known to be strongly influenced by the amount and type of alloying elements and interstitial impurities [2–4]. For example, the yield strength and ductile–brittle transition temperature tend to increase with increasing amount of alloying elements such as Ti and Cr. Under fusion nuclear reactor environments, the vanadium alloys are shown to undergo mechanical property degradation induced by neutron irradiation, and generated hydrogen and helium in a wide temperature range [2,4]. Major efforts have been made to examine how the addition of alloying elements influences the susceptibility of the V alloys to the various embrittlement. Moreover, recent studies [5–7] have indicated that intergranular segregation of impurities like S produces a detrimental effect on the ductility and fracture toughness due to grain boundary weakening in several V alloys. Thus, there is a need to examine the role of segregated impurities in controlling the fracture behavior in irradiated, hydrogenated and helium containing vanadium alloys to develop better vanadium alloys.

The present study is undertaken to examine the effect of neutron irradiation (9.8×10^{24} n/m^2: $E > 0.1$ MeV at 438°C) on the deformation and fracture behavior in three V–20 wt% Ti alloys undoped and individually doped with P or S using a small punch (SP) testing technique. Changes in the grain boundary composition induced by the irradiation are studied by a selected area analysis of scanning

* Corresponding author. Tel.: +1-515 294 7231; fax: +1-515 294 8727; e-mail: kameda@ameslab.gov.

[1] Present address: Department of Die and Mold Design, Chonju Technical College, Chonju 560-760, South Korea.

PII S0022-3115(97)00328-0

Auger microprobe (SAM). The irradiation effect on the fracture properties is elucidated by the impurity segregation and precipitation as well as hardening.

2. Experimental procedure

The materials used in this study were three types of V–20 wt% Ti alloys undoped and individually doped with P or S. The undoped, P-doped and S-doped alloys are designated as UND, PD and SD. The chemical composition of the alloys is shown in Table 1. All the alloys contained different levels of residual C and O in an uncontrolled manner and the SD alloy had the highest content of C and O. Ingots of the alloys were prepared using an electron beam melting method and subsequently rolled at 22°C or about 500°C down to a thickness of about 0.6 mm. Disk-shaped SP specimens with a diameter of 8 mm were punched out from the rolled alloys. The SP specimens of the UND and impurity-doped (PD and SD) alloys were recrystallized at 1170°C and 1230°C for 2 h. All the recrystallized alloys were then annealed at 600°C for 2 h. The recrystallization and annealing treatments were followed by furnace cooling. The resulting grain size of the alloys varied from 110 to 160 μm depending on the SP specimen.

SP specimens, which had been stacked in a lithium-filled TMZ container, were irradiated by fast neutrons at 438°C for 2120 h using the EBR-II reactor. The stacked SP specimens (about 20 mm long) were subjected to the neutron fluence ranging from 9.3 to 10.3×10^{24} n/m^2 ($E > 0.1$ MeV). The average fluence was 9.8×10^{24} n/m^2. Irradiated SP specimens were cooled down to radioactivity levels low enough to be handled safely. Since irradiated alloys were damaged due to lithium attack, the damaged surface (10–20 μm) of the irradiated SP specimen was removed using emery paper (grit 600). Some SP specimens with the surface damage were also prepared. The thickness of the unirradiated and irradiated SP specimens was reduced to 0.5 mm.

SP specimens were set into specially designed specimen holders consisting of lower and upper dies and four clamping screws [8]. A puncher with a hemispherical tip with a diameter of 2.4 mm was used during SP loading. SP tests on unirradiated and irradiated specimens were carried out using a screw driven Instron testing machine in a temperature range from −196°C to 85°C. Load vs. deflection curves were recorded during the punch loading at a cross head speed of 2×10^{-5} m/s. In SP tests, it has been shown [9,10] that the equivalent strain (ε) can be given by

$$\varepsilon(\%) = 12(\delta/t_0)^{1.72}, \quad (1)$$

where t_0 is the SP specimen thickness and δ the deflection. The cracking behavior of load-interrupted and fractured SP specimens was examined using scanning electron microscopy (SEM).

Notched SAM specimens were machined from the undeformed portion of SP specimens tested. SAM specimens were fractured by impact loading below −100°C in an ultra high vacuum chamber of 2×10^{-8} Pa. Selected area SAM analysis was performed on fracture surfaces of the unirradiated and irradiated alloys using Physical Electronics model 660 with a cylindrical mirror analyzer operated at 5 keV. The first derivative peak height ratio (PHR) of various elements, i.e., P_{120}, S_{152}, C_{272}, O_{510} and Ti_{374} to

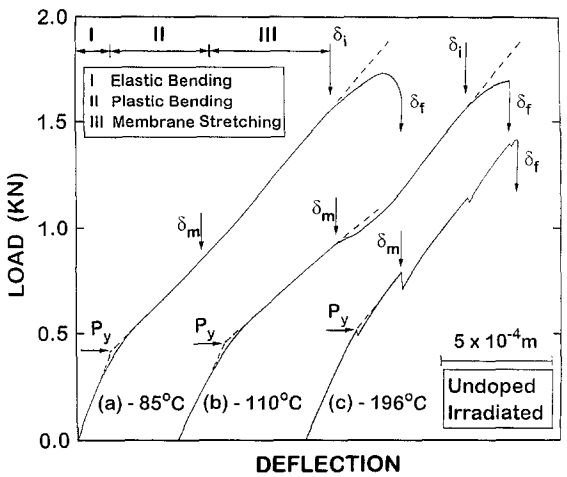

Fig. 1. Load vs. deflection curves obtained from SP tests on irradiated undoped (UND) alloys at (a) −85°C, (b) −110°C and (c) −196°C together with various SP deformation regimes. A loading rate change and a series of load drop can be observed in Fig. 1(b) and (c), respectively. The yield load is represented by P_y. The critical deflection required for the microcrack formation, the macrocrack initiation and propagation are depicted by δ_m, δ_i and δ_f, respectively.

Table 1
Chemical composition of V–20 wt% Ti alloys undoped and doped with P or S (wt%)

	Ti	C	N	O	P	S	H
Undoped alloy (UND)	19.3	0.0116	0.0048	0.0286	0.0009	< 0.0010	0.0013
P-doped alloy (PD)	19.9	0.0061	0.0038	0.0249	0.0300	< 0.0010	0.0012
S-doped alloy (SD)	19.6	0.0140	0.0063	0.0335	0.0020	0.0025	0.0028

V_{478}, normalized by the relative sensitivity factor is given by

$$\text{Normalized PHR} = I_e S_v / I_v S_e, \quad (2)$$

where I_e and S_e are the first derivative peak height and relative sensitivity factor of the individual elements, and I_v and S_v indicate the values of vanadium. The average normalized PHR was determined by taking 25–50 data points on individual grain boundary facets. Since the primary O_{510} and minor V_{509} peaks overlap each other, the peak height of O_{510} was estimated by subtracting the contribution of the minor V_{509} peak, which is 0.23 of the V_{478} peak. The magnitude of segregated impurities is represented by the normalized PHR. The composition of precipitates (C_e) is estimated using an equation of C_e (at.%) $= 100 I_e/S_e/\Sigma(I_i/S_i)$ [11]. Intergranular and transgranular fracture surfaces were sputtered in Ar atmosphere (5×10^{-6} Pa) at 3 keV to determine a depth profile of the elements.

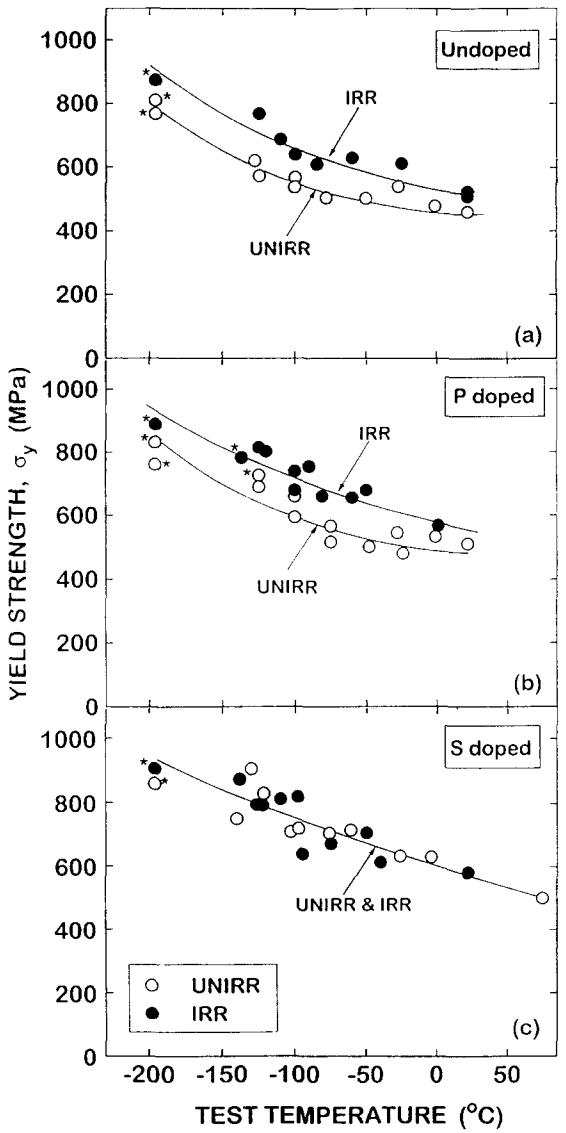

Fig. 2. Comparison of temperature dependence of yield strength (σ_y) in unirradiated (UNIRR) and irradiated (IRR) alloys: (a) undoped (UND), (b) P-doped (PD) and (c) S-doped (SD) alloys. An asterisk indicates yield strength controlled by twinning.

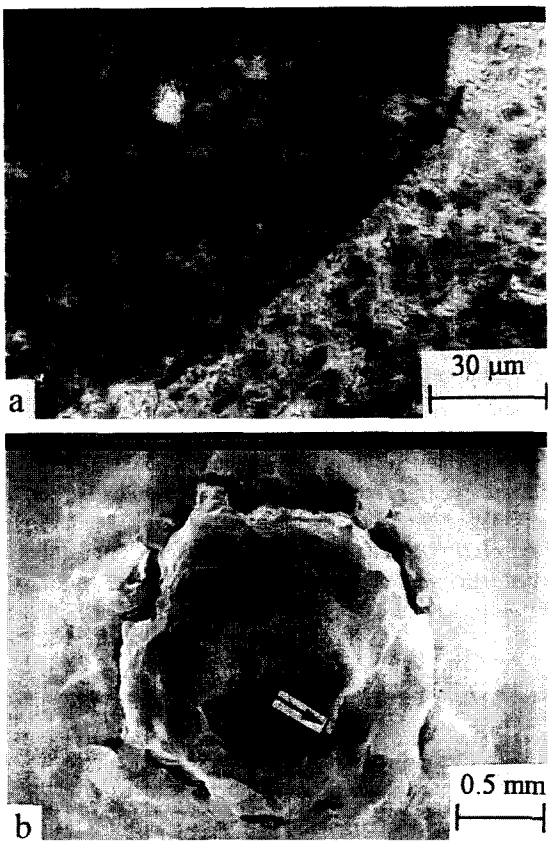

Fig. 3. Cracking morphologies observed in irradiated undoped (UND) SP specimen (a) load-interrupted ($\delta_{int} = \delta_m = 0.65$ mm) and (b) fractured at −85°C. An arrow indicates nucleated microcrack during early deformation.

3. Results

3.1. Mechanical properties

Several load vs. deflection curves in SP tests on irradiated UND alloys at various testing temperatures are shown in Fig. 1. The flow curves were reconstructed from SP tests which had been load-interrupted at several deformation stages to examine the cracking behavior. These results represent the typical SP flow curves observed in the V alloys [12]. The SP deformation behavior during punch loading is divided into (I) elastic bending, (II) plastic

bending and (III) membrane stretching regimes indicating an increase in the load carrying capacity (Fig. 1(a)). The yield load (P_y) was determined at the transition point from the elastic to plastic bending regime, as shown in Fig. 1. The regime III is followed by a change in the loading rate at δ_i and an abrupt load drop at δ_f. A discrete drop in the loading rate, reflected by the formation of microcracks, appeared at δ_m prior to δ_i at -110°C (Fig. 1(b)). A series of load drop caused by twinning or microcracking proceeded in the flow curve at very low temperatures (Fig. 1(c)).

The temperature dependence of the yield strength (σ_y) was estimated from the value of P_y in the unirradiated and irradiated alloys (Fig. 2) [9]. In this figure, the deformation behavior controlled by twinning is indicated by an asterisk. The tensile test result at 22°C in unirradiated UND alloys showed good agreement with the SP result [7]. For the unirradiated alloys, the yield strength became higher in the order of UND, PD and SD alloys. Neutron irradiation-induced hardening occurred in the UND and PD alloys but not in the SD alloy. Unirradiated and irradiated SD alloys had the highest yield strength among the variously treated alloys. The magnitude of the hardening observed in the UND and PD alloys was nearly identical and independent of the testing temperature. This suggests that the irradiation-induced hardening would arise from the formation of defect clusters but not from the precipitation.

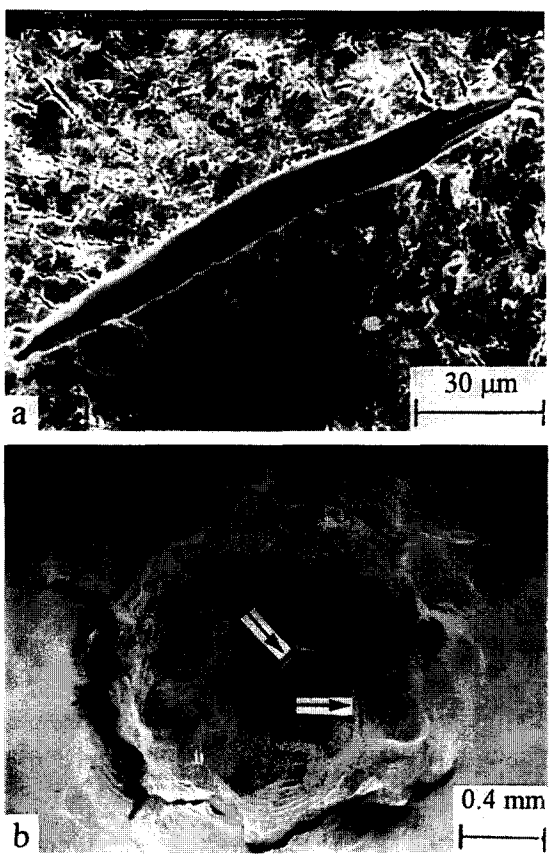

Fig. 4. Cracking morphologies observed in irradiated undoped (UND) SP specimen (a) load-interrupted ($\delta_{int} = 1.0$ mm) and (b) fractured at -110°C. Arrows indicate nucleated microcracks during early deformation.

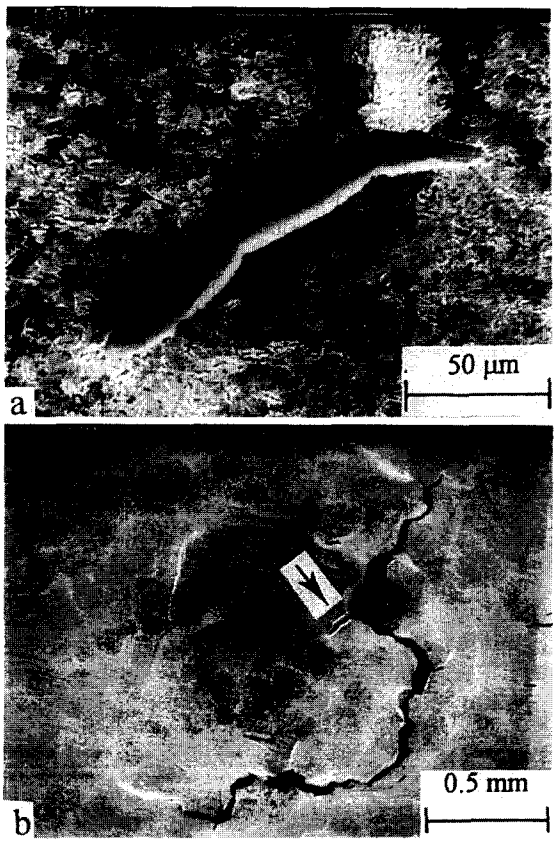

Fig. 5. Cracking morphologies observed in irradiated undoped (UND) SP specimen (a) load-interrupted ($\delta_{int} = 0.5$ mm) and (b) fractured at -196°C. An arrow indicates the linkage of nucleated microcrack to the macrocrack extension.

The cracking behavior was examined in deformed SP specimens. SEM micrographs of the irradiated UND specimens load-interrupted and fractured at -85°C, -110°C and -196°C are shown, respectively, in Figs. 3–5 (each corresponding to the flow curve shown in Fig. 1(a)–(c)). As shown in Fig. 3(a)–Fig. 5(a), the onset of grain boundary microcracks occurred during an early stage of deformation near the center region. It is apparent that the microcrack formation caused the loading rate or load to drop at lower temperatures (Fig. 1(b) and (c)) but not at higher temperatures (Fig. 1(a)). When no discrete changes in the loading rate and the load drop caused by either twinning or microcracking appeared in the flow curve, the value of δ_m was estimated by SEM observation on load-interrupted SP specimens (Fig. 1(a) and (c)) [12]. After further deforming

specimens, macrocracks were found to form at δ_i and extend along the tangential direction, eventually leading to a sudden load drop at δ_f. Microcracks and macrocrack were not linked to each other in all the alloys except the irradiated UND specimen tested at −196°C (Fig. 3(b)–Fig. 5(b)). Similar cracking behavior was observed in most of the alloys [12]. However, the unirradiated UND alloy indicated no microcracking [12] and unirradiated PD alloys revealed many surface cracks (Fig. 6).

The ductility (ε_f) and the critical strain required for the onset of grain boundary microcracks (ε_m) were determined from the values of δ_f and δ_m, respectively, using Eq. (1). The results for the unirradiated and irradiated alloys are plotted against the test temperature in Fig. 7. It is evident that the formation of intergranular microcracks in the UND alloy was made easier by the neutron irradiation. The ductility controlled by the macrocrack propagation decreased to some extent during the irradiation but remained higher than 30% even at −196°C. The irradiated SD alloy revealed two sets of ε_m and ε_f: one group maintained the same ε_m and ε_f as the unirradiated one and the other exhibited easy initiation of microcracks and ductility loss.

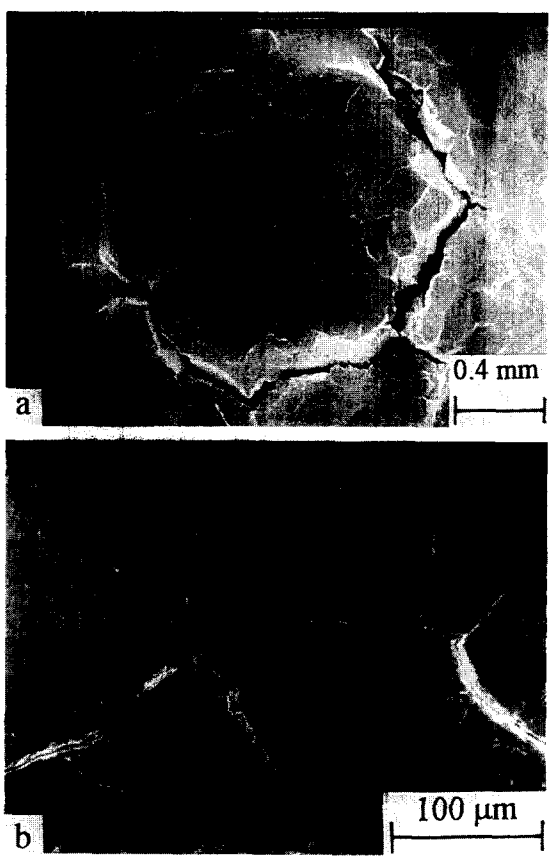

Fig. 6. Cracking morphology observed in unirradiated P-doped (PD) specimen fractured at −125°C: (a) low and (b) high magnification.

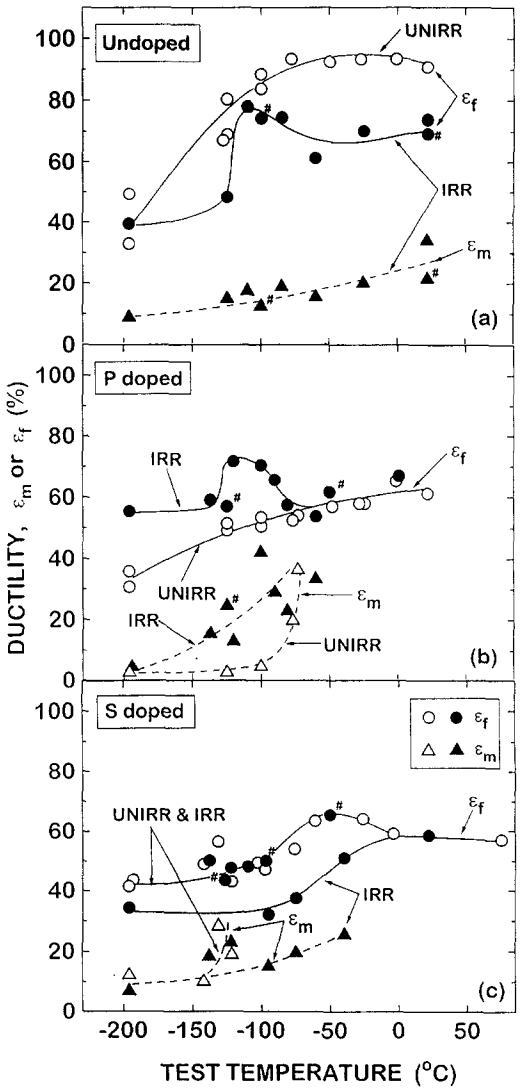

Fig. 7. Comparison of temperature dependence of ductility (ε_f) and critical strain required for microcrack formation (ε_m) in unirradiated (UNIRR) and irradiated (IRR) alloys: (a) undoped (UND), (b) P-doped (PD) and (c) S-doped (SD) alloys. # indicates the result of SP tests on irradiated specimens with surface damage.

In the PD alloy, the irradiation unexpectedly suppressed microcracking and resulted in an increase in the ductility below −90°C. Several other points are summarized: (1) peaks of ε_f emerged at −120°C in the irradiated UND and PD alloys and at −50°C in the SD alloy although the reason is not clear; (2) the presence of surface damage (data points with # in Fig. 7) did not affect the values of ε_m and ε_f; (3) the ductility obtained from the tensile and SP tests at 22°C on the unirradiated UND alloy agreed with each other [7].

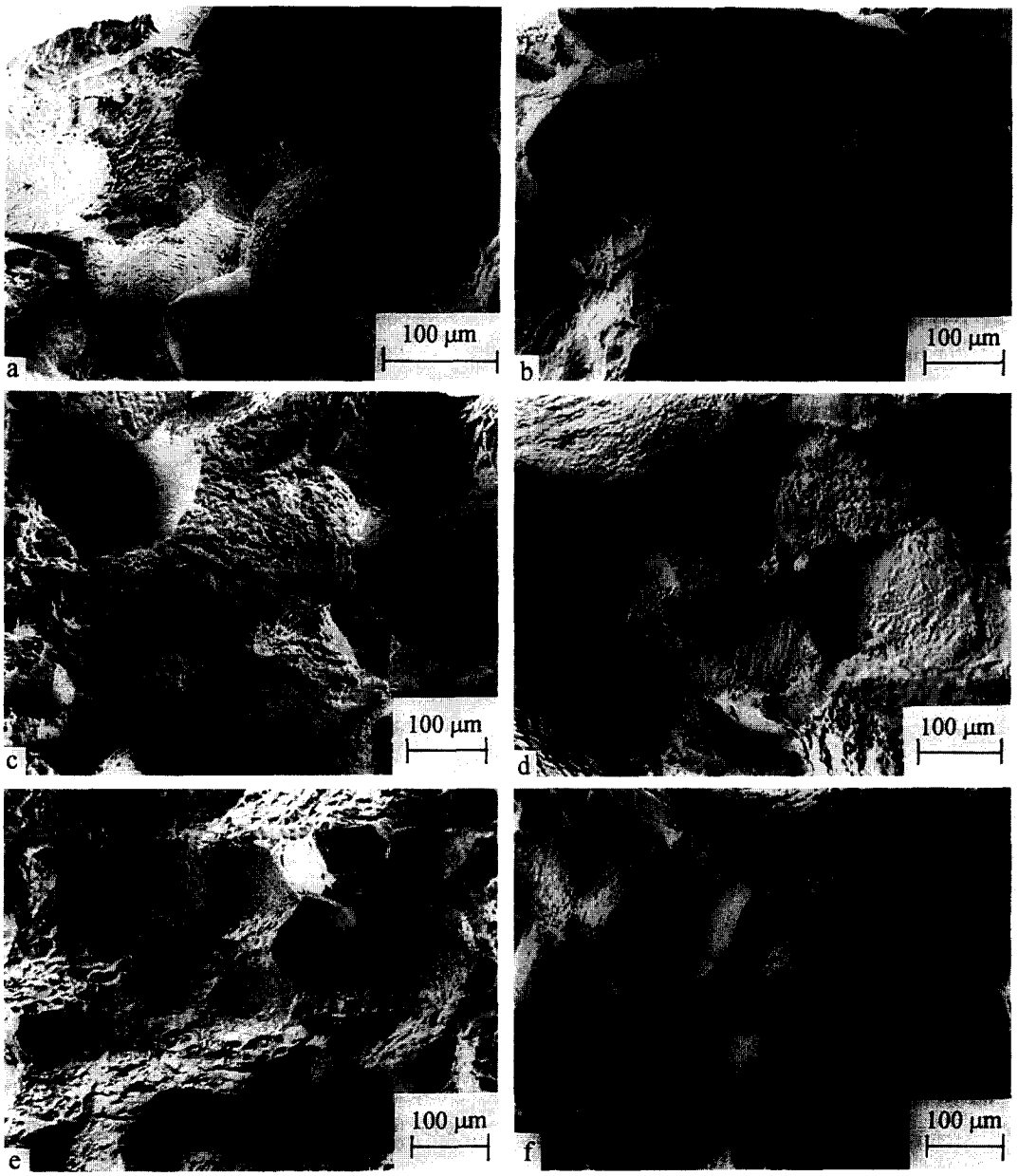

Fig. 8. SEM micrographs of fracture surfaces obtained by SAM impact tests on (a) unirradiated and (b) irradiated undoped (UND) alloys, (c) unirradiated and (d) irradiated P-doped (PD) alloys, and (e) unirradiated and (f) irradiated S-doped (SD) alloys.

SEM fractography of SAM specimens broken by impact loading below −100°C is shown in Fig. 8. All the unirradiated and irradiated alloys depicted a mixture of intergranular and transgranular fracture. The transgranular cracking is due to microvoid coalescence. The unirradiated PD alloy exhibited more transgranular fracture than the unirradiated and SD UND alloys. The neutron irradiation tended to promote intergranular cracking in the vanadium alloys. It must be pointed out [12] that the irradiated SD alloy maintained the same fracture morphology despite the ductility variation.

3.2. Grain boundary composition

The enrichment of S, P, C, O and Ti was identified on intergranular fracture surfaces of the unirradiated and irradiated alloys by the selected area SAM analysis. The dispersion of coarse S or P rich precipitates was detected on transgranular fracture surfaces of the impurity-doped alloys [12]. Argon sputtering experiments on the intergranular fracture surface demonstrated that most of segregated S, P, C, O and Ti was within a monolayer (Fig. 9(a)) [12]. However, deeper profiles of C and Ti were found below

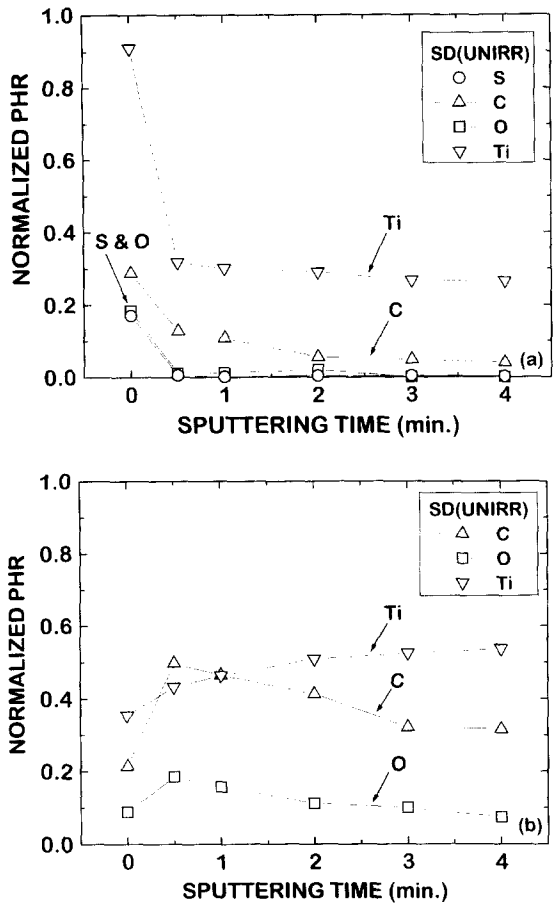

Fig. 9. Depth profiles of (a) S, C, O and Ti on intergranular fracture surface and (b) C, O and Ti on transgranular fracture surface in unirradiated S-doped (SD) alloys.

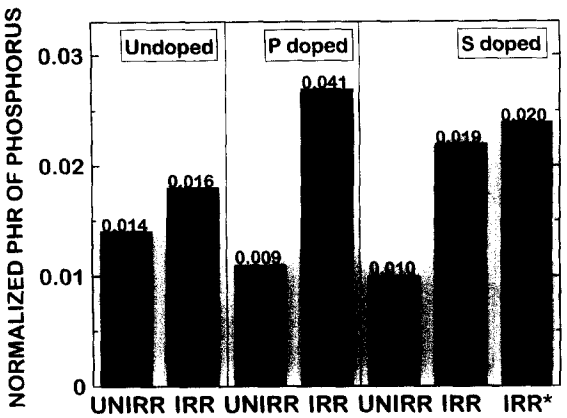

Fig. 11. Comparison of average normalized peak height ratio (PHR) of P in various unirradiated (UNIRR) and irradiated (IRR) alloys. The number on the top of bars indicates the standard deviation. Note that two sets of data are obtained from irradiated S-doped (SD) alloy and an asterisk indicates the data taken from SP specimens showing ductility loss.

the intergranular fracture surface, which are indicative of Ti rich carbides. The depth profile of C, O and Ti on the transgranular fracture surface indicates the presence of Ti rich carbides and oxides in the grain matrix (Fig. 9(b)) [12].

Figs. 10–14 depict the average normalized PHR of S, P, C, O and Ti over 25–50 fractured grain boundary facets of the unirradiated and irradiated alloys. The standard deviations are shown on the top of the bars in these figures. The standard deviation of S and P was comparable to the average value. This means that heterogeneous impurity segregation reflected by the different grain boundary

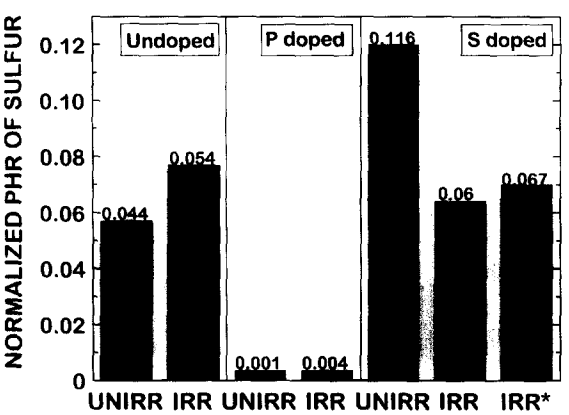

Fig. 10. Comparison of average normalized peak height ratio (PHR) of S in various unirradiated (UNIRR) and irradiated (IRR) alloys. The number on the top of bars indicates the standard deviation. Note that two sets of data are obtained from irradiated S-doped (SD) alloy and an asterisk indicates the data taken from SP specimens showing ductility loss.

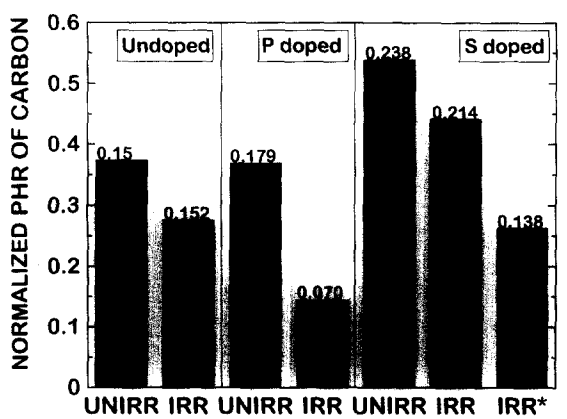

Fig. 12. Comparison of average normalized peak height ratio (PHR) of C in various unirradiated (UNIRR) and irradiated (IRR) alloys. The number on the top of bars indicates the standard deviation. Note that two sets of data are obtained from irradiated S-doped (SD) alloy and an asterisk indicates the data taken from SP specimens showing ductility loss.

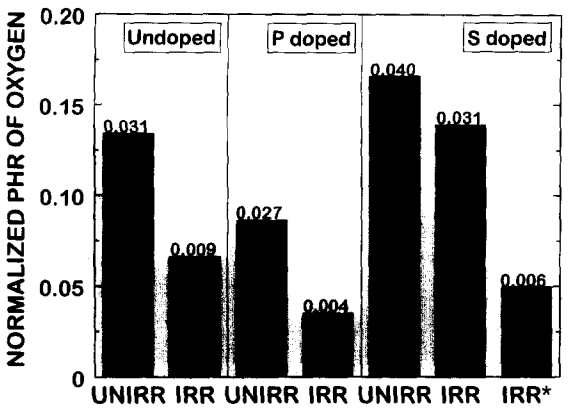

Fig. 13. Comparison of average normalized peak height ratio (PHR) of O in various unirradiated (UNIRR) and irradiated (IRR) alloys. The number on the top of bars indicates the standard deviation. Note that two sets of data are obtained from irradiated S-doped (SD) alloy and an asterisk indicates the data taken from SP specimens showing ductility loss.

structure occurs in the V alloy. Two sets of SAM data were measured in the SD specimens with and without irradiation-induced ductility loss. The asterisk indicates the SAM results for the irradiated SD specimen with ductility loss. The unirradiated SD alloy showed a twofold increase in segregated S over the unirradiated UND alloy (Fig. 10). The neutron irradiation exerted opposite effects on the intergranular S segregation in the UND and SD alloys. The S segregation slightly increased during the irradiation in the UND alloy whereas it decreased by 40% in the SD alloy. However, the unirradiated and irradiated PD alloys had negligible S segregation. Doping P did not enhance the P segregation in the unirradiated alloys and the irradiation

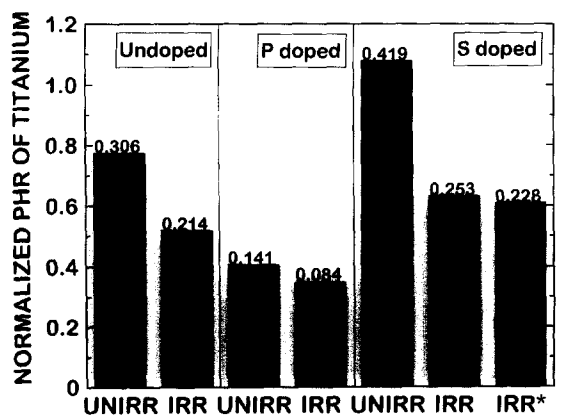

Fig. 14. Comparison of average normalized peak height ratio (PHR) of Ti in various unirradiated (UNIRR) and irradiated (IRR) alloys. The number on the top of bars indicates the standard deviation. Note that two sets of data are obtained from irradiated S-doped (SD) alloy and an asterisk indicates the data taken from SP specimens showing ductility loss.

produced more P segregation in the impurity-doped alloys than in the UND alloy (Fig. 11). The vanadium alloys showed much smaller P segregation, compared to the S segregation observed in the UND and SD alloys (Figs. 10 and 11). In the unirradiated alloys, the grain boundary content of C and O varied in a similar trend to the bulk and the Ti content also changed despite the constant bulk composition (Figs. 12–14). The irradiation led to a reduction in the grain boundary content of C, O and Ti in all the alloys and the grain boundaries in the irradiated PD alloy possessed the smallest amount of C, O and Ti. Furthermore, it should be noted that the SD specimen with ductility loss induced by the irradiation revealed smaller grain boundary contents of C and O than that not affected by the irradiation (Figs. 10–14). However, the amount of S, P and Ti at grain boundaries remained the same independent of the ductility variation in the irradiated SD specimens.

The compositions of coarse phosphides and sulfides dispersed on the transgranular fracture surface of the PD and SD alloys are shown, respectively, in Fig. 15(a) and (b). It is clear that the phosphide and sulfide contained

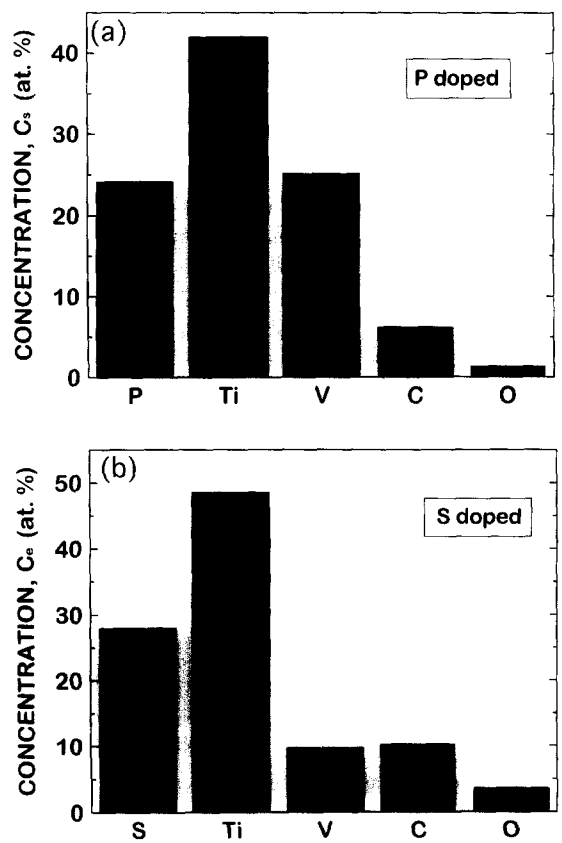

Fig. 15. Chemical compositions of (a) phosphides and (b) sulfides observed in the P-doped (PD) and S-doped (SD) alloys, respectively.

large amounts of Ti. It was found [12] that the irradiation did not affect the dispersion of the coarse precipitates and the density of the phosphides and sulfides was not much different in the impurity-doped alloys despite the different bulk content of P and S.

4. Discussion

By means of the SP testing method and SAM analysis, the present study has shown how neutron irradiation (9.8×10^{24} n/m^2: $E > 0.1$ MeV at 438°C) influences the mechanical properties and grain boundary composition in the three V–20 wt% Ti alloys, undoped, P-doped and S-doped all containing residual C and O. The neutron irradiation produced a deleterious or beneficial effect on the ductility in the V alloys. Intergranular segregation and desegregation of impurities were induced by the irradiation depending on the type of alloys and impurities. In this section, the rationale for the irradiation effect on the fracture properties is given by the impurity segregation and precipitation as well as the hardening behavior. The variations in the grain boundary composition induced by the irradiation are interpreted in light of the dynamic interaction between impurity and defect fluxes and the impurity solubility.

In order to account for the irradiation effect on the fracture properties in the V–20 wt% Ti alloys, intergranular cracking mechanisms are briefly presented. As schematically illustrated in Fig. 16, grain boundary microcracks nucleate at precipitates along grain boundaries due to the pileup of dislocations and then propagate under a biaxial loading mode by expending the grain boundary cohesive energy and plastic work. Thus three factors, i.e., grain boundary precipitation, impurity segregation and hardness, which are affected by the irradiation, would dominantly control the intergranular fracture. In iron base alloys, it is shown [13,14] that the segregation of S with higher electronegativity more strongly reduces the grain boundary cohesion than that of P, and the C segregation conversely gives rise to grain boundary toughening. These findings would be applied to the V alloys although the role of segregated oxygen is not clear. The grain boundary cohesion would highly vary due to a wide distribution of the impurity segregation in the V alloys. Thus two types of cracking were observed: (1) grain boundary microcracks heterogeneously initiated at lower strains below 30%, which propagated a limited distance; (2) macrocrack propagation governing the ductility occurred in mixed intergranular and transgranular modes along the tangential direction.

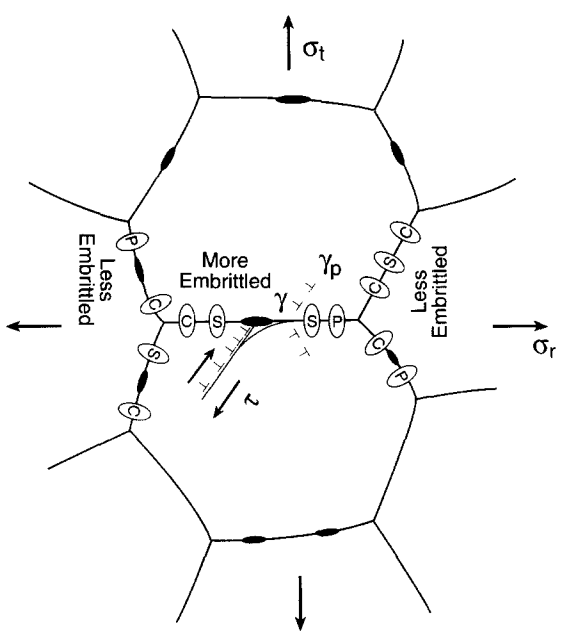

Fig. 16. Schematic representation of onset of brittle cracks along grain boundaries with segregated and precipitated impurities.

The irradiation effect on the mechanical properties and grain boundary composition in the vanadium alloys undoped and doped with impurities is summarized in Table 2. In the irradiated UND alloy, the grain boundary cohesion and dislocation activity would be reduced as a result of the S and P segregation and the C desegregation as well as the hardening. Thus brittle microcracks would readily form at grain boundaries with larger amounts of segregated S and P and/or smaller amounts of segregated C in the irradiated UND alloy [15]. However, the nucleated microcrack would not be able to grow extensively along contiguous grain boundaries with higher cohesion at lower strain levels. In addition, microvoid coalescence, leading to transgranular cracking, would not easily occur in the UND alloy without coarse incoherent precipitates. Hence the ductility controlled by a mixture of intergranular and transgranular cracking did not drop as much as expected from the easy formation of microcracks in the irradiated UND alloy.

The fracture properties in the impurity-doped alloys were influenced by the irradiation in a more complex manner. It was found that some irradiated S-doped specimens showed ductility loss and others did not (Fig. 7). In the SD alloy, the irradiation induced the P segregation and reduced the grain boundary content of S, C, O and Ti (Figs. 10–14 and Table 2). Moreover, the SD specimen showing irradiation-induced ductility loss had a smaller grain boundary content of C than that not affected by the irradiation while both maintained the same amount of S, P and Ti at grain boundaries. This implies that the irradiation would cause a change in segregated C but not in Ti rich carbides at grain boundaries in the SD alloy. Thus it is most likely that the ductility loss in the irradiated SD specimen would be ascribed to a larger reduction of segregated C producing a weaker toughening effect. In the irradiated SD specimen with the larger content of C, the

Table 2
Summary of the irradiation effect on the mechanical properties and grain boundary composition in various V alloys

	Undoped alloy	P-doped alloy	S-doped alloy
Ductility	decrease	increase	decrease none
Hardening	yes	yes	none
S segregation	small increase	none	large decrease
P segregation	small increase	medium increase	medium increase
C content	small decrease	large decrease	large decrease small decrease
Ti content	medium decrease	small decrease	large decrease

toughening effect induced by the S desegregation would offset against the embrittling effect due to the small P segregation and C desegregation, thereby exerting no irradiation effects on the ductility.

On the contrary, the irradiation enhanced the ductility at low temperatures in the PD alloy (Fig. 7) although it produced the P segregation, the C desegregation and the hardening (Table 2). This unexpected result would be related to the finding that the irradiated PD alloy had the smallest grain boundary content of C, O and Ti (Figs. 12–14). That is, the irradiation would reduce not only the C and O segregation but also the density of grain boundary precipitates, being crack nuclei. Thus crack nucleation would become more difficult than crack propagation along grain boundaries in the irradiated PD alloy with negligible segregated S, thereby improving the ductility controlled by the crack nucleation. Furthermore, in the impurity-doped alloys, the dispersion of incoherent precipitates would promote the nucleation and coalescence of microvoids regardless of the irradiation effect, leading to lower ductility at higher temperatures than the UND alloy.

The underlying mechanisms controlling the grain boundary composition during irradiation are taken into account in light of the defect/impurity interaction affecting the impurity flux and the grain boundary capacity of segregated impurities. During neutron irradiation, some of the interstitials and vacancies migrate to grain boundaries for their annihilation. The dynamic interaction of defects with impurities during the neutron irradiation would cause the grain boundary composition to change. It is shown in irradiated materials [16–19] that intergranular impurity segregation is driven by forming mobile interstitial–impurity pairs and impurity concentration gradients while impurity desegregation is controlled by vacancy annihilating fluxes, i.e., inverse Kirkendall effect. S and P regarded as undersized substitutional impurities in the vanadium alloy would interact with both interstitials and vacancies [20]. The segregation and desegregation of S and P are expected to occur during the irradiation depending on the relative strength of impurity fluxes via interstitials, concentration gradients and vacancies near grain boundaries (Fig. 17) [21].

It is possible that irradiation would affect the capacity of grain boundaries to absorb impurities by changing the impurity solubility. The grain boundary enrichment of impurities is well known to be inversely related to the solubility [22]. Guttmann and McLean [23] have suggested that the precipitation and grain boundary segregation of impurities would be analogous and simultaneous consequences. As schematically illustrated in Fig. 18(a) and (b), increasing the free energy of bulk precipitates enhances the impurity solubility while increasing the free energy of segregated boundaries reduces the impurity segregation and vice versa. A reduction in the impurity solubility facilitates the precipitation and segregation by repelling foreign atoms. By applying hypothetically the free energy in irradiated materials, it is shown [24] that irradiation destabilizes undersized precipitates by increasing the free energy of the precipitates and conversely stabilizes oversized ones (Fig. 18(a)). The free energy of segregated boundaries and bulk precipitates would change in a similar trend because of the interaction of defects with segregants and precipitates.

A recent study [25,26] has indicated that the irradiated UND and SD alloys contained considerably lower amounts of segregated S, compared to alloys thermally aging at 438°C for 2120 h (equivalent to the irradiation condition) which maintained the equilibrium segregation. The irradiation would promote the dissolution of undersized Ti rich sulfides, thereby reducing the grain boundary capacity of

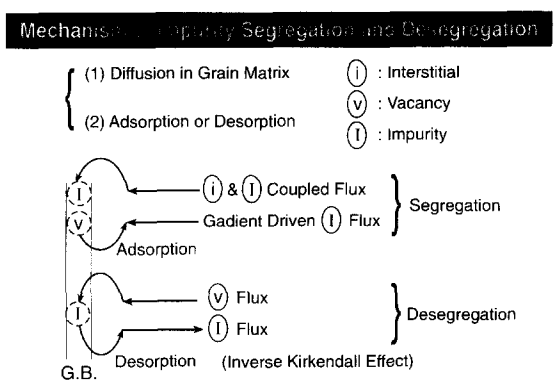

Fig. 17. Schematic illustration of segregation and desegregation fluxes of undersized substitutional impurities via interstitials, concentration gradient and vacancies near grain boundaries during neutron irradiation.

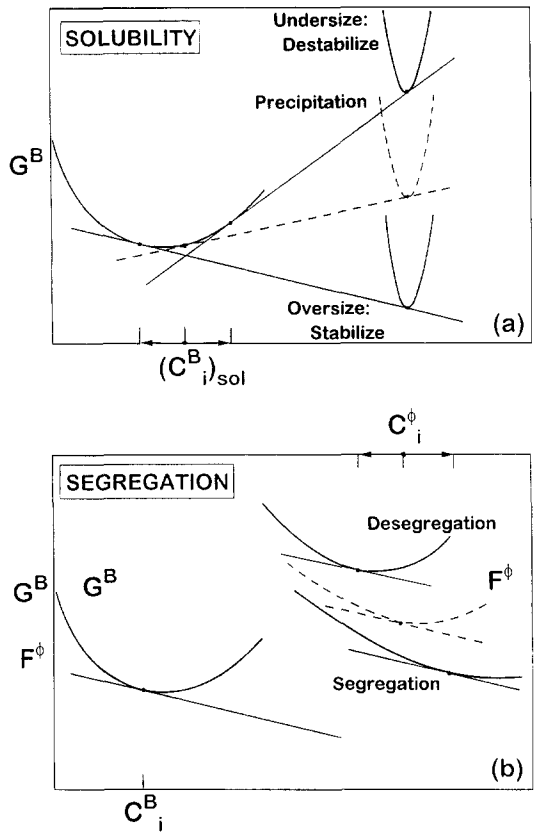

Fig. 18. Influence of stability of bulk precipitate and segregated boundary relative to that of matrix on (a) the solubility and (b) intergranular segregation of impurities. G^B is Gibbs free energy in the bulk and F^ϕ is Hermholz free energy of segregated boundary.

segregated S. This presumption is consistent with the present results that irradiation-induced hardening is controlled by an athermal process in the UND and PD alloys and there is no hardening behavior in the SD alloy. Moreover, the desegregation flux of S assisted by annihilating vacancies would compete and overwhelm the segregation flux via interstitials and/or concentration gradient, respectively, in the UND and SD alloys. The absence of segregated S in the unirradiated, irradiated and thermally aged PD alloys would arise not from the site occupation by segregated P but from the solubility increase because of their small P segregation [25,26].

All the irradiated and thermally aged alloys had much smaller P segregation than the S segregation observed in the UND and SD alloys [25,26]. The dispersion of coarse phosphides in the PD alloy was found similar to that of sulfides in the SD alloy despite higher bulk contents of P in the PD alloy [12]. Thus the vanadium alloy would have higher solubility of P than S. In this way, the grain boundary would not accommodate large P segregation even in the PD alloy. The irradiation would not affect the solubility of P as much as that of S probably because of smaller volume misfit of Ti rich phosphides. Also the role of defects in controlling the P fluxes would be minimal [25].

The neutron irradiation reduced the grain boundary content of C and O, as opposed to the thermal ageing [25,26]. Increasing the free energy of undersized precipitates such as titanium rich carbides or oxides in the irradiated matrix would enhance the solubility of interstitial elements. Thus segregated C and O and precipitates at grain boundaries would be dissolved into the grain matrix during the irradiation. In addition, the irradiated SD alloy had a variation in the irradiation effect on the grain boundary content of C and O. The solubility of C and O heterogeneously would change in the irradiated SD alloy with the large bulk content of C and O due to possible large variations in the precipitation distribution induced by the irradiation.

5. Conclusions

The mechanical properties in unirradiated and neutron irradiated (9.8×10^{24} n/m^2: $E > 0.1$ MeV at 438°C) V–20 wt% Ti alloys, undoped, P-doped and S-doped all containing residual C and O have been studied using a small punch (SP) testing method in conjunction with scanning Auger microprobe analysis on the grain boundary composition. The results obtained in this study are summarized in the following.

(1) Neutron irradiation-induced hardening occurred in undoped and P-doped alloys but not in S-doped alloy. The magnitude of the hardening remained almost the same and was independent of the testing temperature.

(2) The formation of intergranular microcracks, not leading to specimen failure, was promoted by neutron irradiation in all the undoped and some S-doped specimens.

(3) An irradiated undoped alloy had ductility loss to smaller extents than expected from the easy microcracking as a result of mixed modes of intergranular and transgranular fracture.

(4) The S-doped alloy showed variations in the irradiation effect on the ductility. The irradiation produced a beneficial effect on low temperature ductility in the PD alloy.

(5) The neutron irradiation induced intergranular S segregation in the undoped alloy and S desegregation in the S-doped alloy. Unirradiated and irradiated P-doped alloys indicated negligible S segregation.

(6) All the alloys had much smaller P segregation independent of the bulk P content than the S segregation observed in the undoped and S-doped alloys though the irradiation enhanced the P segregation.

(7) The grain boundary content of C, O and Ti in the V alloys was reduced during the irradiation. A large decrease

in the C content affecting the ductility occurred in the irradiated P-doped alloy and S-doped specimens showing ductility loss.

(8) The irradiation effect on the fracture behavior is rationalized by the changes in segregated and precipitated impurities as well as the hardening. The mechanisms of irradiation-induced impurity segregation and desegregation are taken into account in light of the defect/impurity interaction affecting the impurity flux and solubility.

Acknowledgements

Ames Laboratory is operated for the US Department of Energy, Iowa State University under contract No. W-7405-ENG-82. This work was supported by the Office of Basic Energy Sciences, Division of Materials Sciences. The authors wish to thank Drs D.S. Gelles, M.L. Hamilton and A.E. Ermi at Pacific Northwest Laboratory for performing neutron irradiation experiments using the EBR II reactor at the Idaho National Engineering Laboratory. One of the authors (D.Y.L.) is grateful to the Korean Ministry of Education for providing the financial support.

References

[1] D.R. Harris, G.J. Buttermore, A. Hishinuma, F.W. Wiffen, J. Nucl. Mater. 191 (1992) 92.
[2] B.A. Loomis, D.L. Smith, J. Nucl. Mater. 191–194 (1992) 84.
[3] D.L. Harrod, R.E. Gold, Int. Met. Rev. 4 (1980) 163.
[4] D.R. Diercks, B.A. Loomis, J. Nucl. Mater. 141–143 (1987) 1117.
[5] C.V. Owen, W.A. Spitzig, A.J. Bevolo, Mater. Sci. Eng. A 110 (1989) 69.
[6] H. Li, M.L. Hamilton, R.H. Jones, Scripta Metall. Mater. 33 (1995) 1063.
[7] D.Y. Lyu, T.E. Bloomer, Ö. Ünal, J. Kameda, Scripta Mater. 33 (1996) 317.
[8] J.M. Baik, J. Kameda, O. Buck, Scripta Metall. 17 (1983) 1443.
[9] X. Mao, H. Takahashi, J. Nucl. Mater. 150 (1987) 42.
[10] J. Kameda, X. Mao, J. Mater. Sci. 27 (1992) 983.
[11] M.P. Seah, Practical Surface Analysis by Auger and X-ray Photoelectron Spectroscopy, B. Briggs, M.P. Seah (Eds.), Wiley, New York, 1983, p. 181.
[12] J. Kameda, T.E. Bloomer, D.Y. Lyu, unpublished work at Ames Laboratory.
[13] R.P. Messemer, C.L. Briant, Acta Metall. 30 (1982) 457.
[14] K. Abiko, S. Suzuki, H. Kimura, Trans. Jpn. Inst. Metals 23 (1982) 43.
[15] J. Kameda, C.J. McMahon Jr., Metall. Trans. A 11 (1980) 91.
[16] R.A. Johnson, N.Q. Lam, Phys. Rev. B 13 (1976) 4364.
[17] H. Wiedersich, R.P. Okamoto, N.Q. Lam, J. Nucl. Mater. 83 (1979) 98.
[18] S.M. Murphy, J.M. Perks, J. Nucl. Mater. 171 (1990) 360.
[19] D. McLean, Grain Boundaries in Metals, Clarendon, Oxford, 1957.
[20] H.W. King, J. Mater. Sci. 1 (1966) 79.
[21] J. Kameda, C.R. Gold, T.E. Bloomer, Proc. 6th Int. Symp. on Environmental Degradation of Materials in Nuclear Power System–Water Reactors, R.E. Gold, E.P. Simonen (Eds.), The Minerals, Metals and Materials Society, Warrendale, PA, 1993, p. 531.
[22] M.P. Seah, E.D. Hondros, Proc. R. Soc. London A 335 (1973) 191.
[23] M. Guttmann, D. McLean, Interfacial Segregation, C. Johnson, J.M. Blakely (Eds.), ASM, Metals Park, OH, 1979, p. 261.
[24] S.L. Maydet, K.C. Russel, J. Nucl. Mater. 64 (1977) 101.
[25] T.E. Bloomer, D.Y. Lyu, J. Kameda, Microstructure Evolution During Irradiation, T. Diaz de la Rubia, L.W. Hobbs, I.M. Robertson, G.S. Was (Eds.), Material Research Society, Pittsburgh, PA, 1997, p. 545.
[26] J. Kameda, T.E. Bloomer, D.Y. Lyu, 8th Int. Conf. on Fusion Reactor Materials (ICFRM-8), Sendai, Japan, 1997.